Research Article | Vol. 27, No. 18 | 2 Sep 2019 | OPTICS EXPRESS 26203
Optics EXPRESS

Low loss slow light propagation in silicon slot waveguide

DEEPAK V. SIMILI[1,*] AND MICHAEL CADA[1,2]

[1]Department of Electrical and Computer Engineering, Dalhousie University, Halifax, NS B3H 4R2, Canada
[2]IT4Innovations and Nanotechnology Center, VSB-Technical University of Ostrava, 70833 Ostrava-Poruba, Czech Republic
[*]deepak.v.simili@dal.ca

Abstract: Silicon slot waveguide Bragg gratings have been designed, fabricated and the experimental data has been analyzed for its slow light properties. Slow light with a group index of 12.38 at a wavelength near 1555 nm and having a low propagation loss of 5.1 dB/mm has been determined for internally corrugated slot waveguide Bragg gratings on a silicon-on-insulator platform. The combination of slow light and low propagation loss make the internally corrugated slot waveguide Bragg gratings especially attractive as a phase shifter section for low drive voltage, high speed and compact electro-optic modulators.

1. Introduction

Silicon slot waveguides [1] are a key component in active and passive photonic devices to enable development of silicon-based photonic integrated circuits (PIC). It has been used to provide ultra compact, broadband polarization handling for application to large scale PIC's [2], high performance electro-optic modulators [3–6] as well as biosensor applications [7, 8]. Silicon slot waveguide with Bragg gratings [9] offers the possibility of combining advantages in a slot waveguide with functionality of a Bragg grating (BG). Specifically, they are one-dimensional (1D) periodic structures wherein light is confined in the low index slot medium thereby allowing for utilization of optical properties of the low index slot medium and it possesses a stopband which is characteristic of a photonic crystal (PC) structure. Slot waveguide BG structures have been demonstrated for its sensing and resonator based capabilities [9] and has been theoretically investigated for its slow light effects [10]. Enhancement of the in-device electro-optic coefficient (effective r_{33}) of a silicon-organic hybrid electro-optic modulator using slow light effect has been demonstrated in a 1D PC slot waveguide using external corrugations [11]. Although slow light using two-dimensional (2D) PC slot waveguides has been used to greatly enhance the effective r_{33} [12, 13], it suffers from higher propagation loss due to scattering from the 2D PC holes and lower fabrication tolerance due to a more complex arrangement of PC holes as in the case of dispersion engineered PC slot waveguides [12] . It has been reported that the propagation loss for a 2D PC slot waveguide is sensitive to roughness in the hole surface and slot width [14]. The advantage of 1D PC slot waveguides considered in this work over 2D PC slot waveguides is that it has lower fabrication complexity and potential for lower propagation loss [11].

In this paper we explore slow light capabilities of silicon slot waveguide BG structures through design, fabrication and experimental data analysis. The slot waveguide BG structure is introduced in a Mach Zehnder Interferometer (MZI) circuit which is used to extract group indices and insertion loss in the slow and fast light regimes within 1.5-1.6 μm wavelength range through simulation and experimental data. This is followed by device application analysis of the proposed slot BG waveguide as a phase shifter section for an electro-optic (E-O) modulator with an E-O polymer cladding.

#369070 https://doi.org/10.1364/OE.27.026203
Journal © 2019 Received 3 Jun 2019; accepted 1 Jul 2019; published 30 Aug 2019

Optics EXPRESS

2. Modeling and simulation

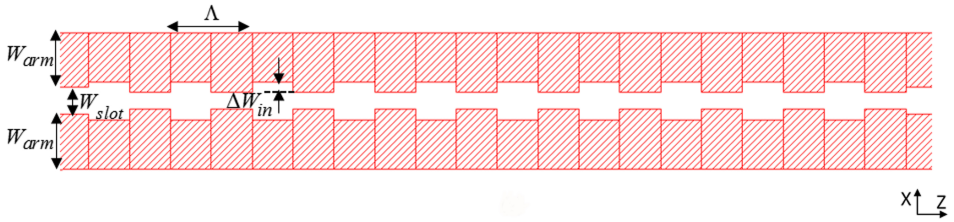

Fig. 1. kLayout screen capture of silicon slot waveguide BG section with Internal corrugations.

The fundamental unit in a slot waveguide BG structure is the slot waveguide which has an arm width (W_{arm}) and a slot gap (W_{slot}) as shown in Fig. 1. The geometry of a uniform slot waveguide BG structure with internal corrugations is shown in Fig. 1 where Λ is the Bragg period, ΔW_{in} is the internal corrugation width.

The theoretical photonic band structure of the fundamental quasi TE mode for a unit cell of the internally corrugated slot waveguide BG with ΔW_{in} = 20 nm is shown in Fig. 2(a). We can observe flattening of the mode close to the band edge indicating slow propagating light. The optical mode is strongly confined in the low index slot medium with a confinement factor (σ) of 0.36 as shown in Fig. 2(b).

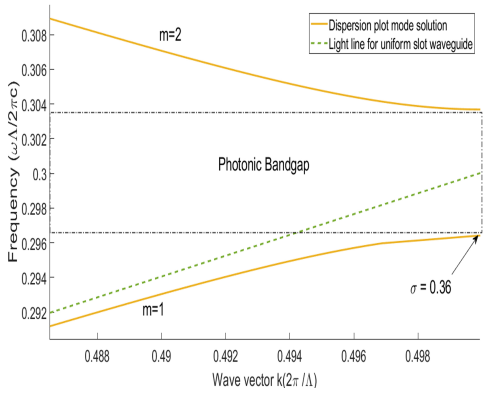

(a)

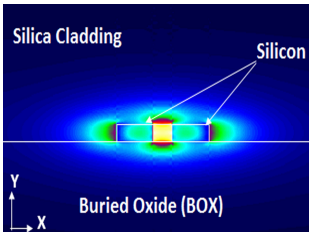

(b)

Fig. 2. (a) Photonic band structure for internal corrugated slot waveguide with ΔW_{in} = 20 nm. (b) TE mode profile at the band edge for the fundamental mode band (m=1), where the optical mode confinement factor (σ) is 0.36 in the slot region.

Optics EXPRESS

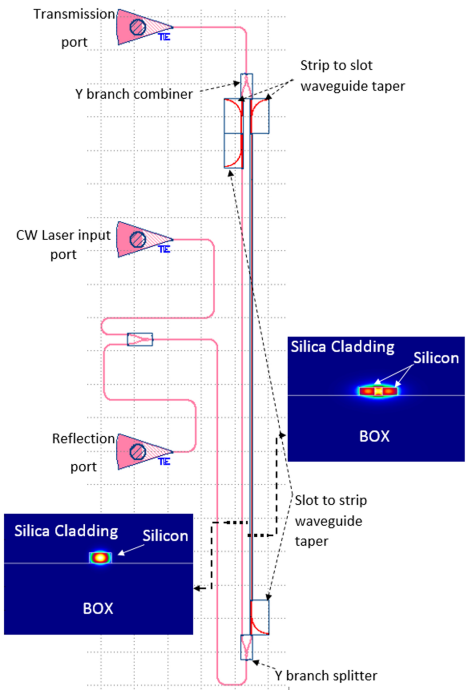

(a)

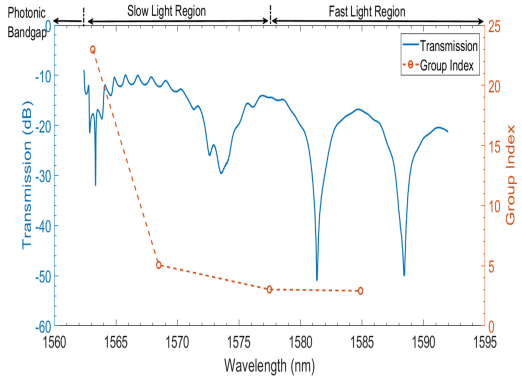

(b)

Fig. 3. (a) kLayout screen capture of MZI circuit along with strip waveguide and slot waveguide cross sections in two arms with fundamental quasi-TE mode intensity plots. (b) Simulated transmission spectrum for ΔW_{in} = 20 nm along with calculated group index.

2.1. *Photonic circuit simulation*

Mask layout screen capture of the MZI photonic circuit with a slot waveguide BG section in one of the arms is shown in Fig. 3(a). The two MZI arms have the same length with difference being one arm has a slot waveguide BG section and the other arm has a strip waveguide section. Both the arms have strip to slot waveguide tapers to cancel the effect of each other. Thus, the resulting transmission spectrum from the MZI would be a combination of the strip waveguide properties and the slot waveguide BG section. With group index of the strip waveguide experimentally determined to be 4.19 in the wavelength region of 1.52-1.58 μm, group index of the slot waveguide BG section can be extracted out in this wavelength region.

In order to get a realistic simulation , the circuit in Fig. 3(a) is simulated using Lumerical INTERCONNECT which is a commercial photonic circuit simulation software tool. Photonic circuit simulation is an important step in the design flow of photonic integrated circuits (PIC) as one can optimize an individual component by performing several iterations and variations and then integrate the component in the circuit so that it performs as intended [15].

The slot waveguide arm width is chosen as 200 nm , with a slot gap of 100 nm. The Bragg period is 460 nm so that the stopband edge is within 1.5-1.6 μm.The number of grating periods considered is 600 which gives the length of the BG section as 276 μm.

The photonic circuit simulation uses a combination of Process Design Kit (PDK) library [16] building block elements that are calibrated based on foundry fabrication process experimental results and custom components whose S parameters are obtained through simulation using computer-aided design (CAD) tools. Specifically, the strip to slot waveguide tapers were modeled

Optics EXPRESS

using 3D FDTD technique and slot waveguide Bragg gratings were modeled using Rigorous Coupled Mode Theory (RCMT). The frequency domain simulation is based on scattering data analysis which is obtained through the physical device or component modeling. Building block elements from the PDK library [16] are Y branch, Input/output grating couplers and the strip waveguide. Custom components used are strip to slot waveguide mode tapers and slot waveguide Bragg gratings.

Simulated transmission spectrum of the photonic circuit is shown in Fig. 3(b). From the transmission spectrum we can observe a variation in the fringe minima. This is because of increase in group index of the slot waveguide BG arm as one approaches with wavelengths close to the photonic bandgap.The group index can be extracted from the transmission spectrum using the relation [17],

$$n_g(\lambda) = \pm \frac{\lambda^2}{[FSR(\lambda)]L} + n_{g(ref.)} \tag{1}$$

Here $n_g(\lambda)$ is the group index of the slot waveguide BG section at a wavelength λ , $FSR(\lambda)$ is the corresponding free spectral range in the MZI transmission spectrum, L is the length of the slot waveguide BG section and $n_{g(ref)}$ is the group index of the reference arm strip waveguide which is experimentally determined to be 4.19 in the considered wavelength range. In the fast light region shown in Fig. 3(b), the group index of the slot waveguide arm is smaller than that of the strip waveguide indicating a shorter optical path length than the strip waveguide arm. As one approaches the slow light region, the group index of slot BG waveguide increases and becomes equal to that of the strip waveguide resulting in broadening of the fringe compared to the fast light region. In the slow light region, the group index of slot BG waveguide is now greater than that of the strip waveguide resulting in greater optical path length in the slot BG waveguide arm. The plus symbol is applied when calculating group index in the slow light region and minus symbol is applied in the fast light region [17]. A peak group index of 22.98 is obtained in the slow light region as shown in Fig. 3(b).

We can observe Fabry-Perot type oscillations due to group index mismatch in the slow light region. This contributes to coupling losses in the slot BG waveguide arm at the slow light wavelength region. Insertion loss for the for the slot waveguide Bragg gratings which includes coupling loss and propagation loss can be estimated from difference in contrast ratios of MZI transmission spectrum fringes in the slow and fast light regimes [17] wherein the positive and negative symbols are used in Eq. (2) respectively.

$$IL(\lambda) = C_p(\lambda) + \alpha_{sw}(\lambda)L \approx \alpha_{fw}L + E_{mean} \pm E(\lambda) \tag{2}$$

where ,

$$E(\lambda) = 20log_{10}(\frac{E_{max}(\lambda) + E_{min}(\lambda)}{E_{max}(\lambda) - E_{min}(\lambda)}) \tag{3}$$

Here $E_{max}(\lambda)$ and $E_{min}(\lambda)$ are maximum and minimum electric fields at the MZI output. E_{mean} is mean value of $E(\lambda)$ in the fast light region, α_{fw} is propagation loss in the fast light region, approximated as 10 dB/cm which is comparable to that of a slot waveguide and L is the length of the slot waveguide BG section which is 276 μm. Taking the ratio to calculate $E(\lambda)$ filters out the effect of the input output grating couplers, 3 dB splitter and combiner and strip to slot mode converters as they are identical for both the MZI arms. This leaves only coupling loss $C_p(\lambda)$ to the slow light mode and propagation loss of slow light (α_{sw}) [17]. Using this technique for the simulated transmission spectrum shown in Fig. 3(b), a phase shifter insertion loss of 4.39 dB at a wavelength of 1563 nm with an extinction ratio of $\sim$ 14 dB is obtained in the slow light region.

Optics EXPRESS

2.2. Fabrication tolerance analysis

In order to understand the effect of manufacturing variability on the central Bragg wavelength, a slot arm width of $+/-10$ nm from the design dimension of 200 nm and a SOI thickness variation of +3.1 to −4.7 nm from the nominal thickness of 220 nm is considered in the analysis. The corresponding slot waveguides had a minimum effective index of 1.611 and maximum effective index of 1.7215 at a wavelength of 1550 nm . This corresponds to a minimum Bragg wavelength of 1482.1 nm and a maximum Bragg wavelength of 1583.7 nm for the designed grating period of 460 nm. This shift in Bragg wavelength from design target due to manufacturing variability can be overcome by having design variants with varying Bragg periods and through thermal tuning. By introducing air trenches through under etching around the MZI arms , thereby providing better thermal isolation, a tuning efficiency of 0.49 mW/FSR has been demonstrated [18]. This corresponds to 0.98-4.9 mW for 2-10 FSR wavelength shifts. For the mask layout preparation, several design variants were considered with varying Bragg periods in order to compensate for fabrication variation.

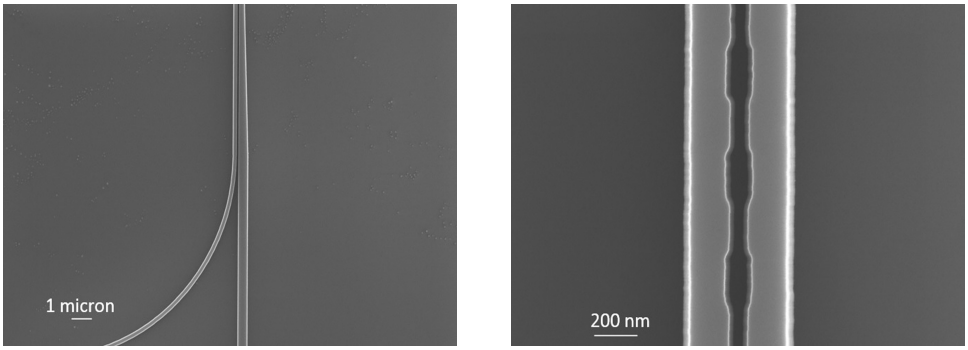

(a) (b)

Fig. 4. (a) Top view SEM image of strip waveguide to slot waveguide mode converter. (b) Top view SEM image of slot waveguide uniform BG with internal corrugation width of ΔW_{in} = 20 nm.

3. Fabrication

The devices were fabricated using 100 KeV Electron Beam Lithography [19]. The fabrication used silicon-on-insulator wafer with 220 nm thick silicon on 3 μm thick silicon dioxide. The substrates were 25 mm squares diced from 150 mm wafers. After a solvent rinse and hot-plate dehydration bake, hydrogen silsesquioxane resist (HSQ, Dow-Corning XP-1541-006) was spin-coated at 4000 rpm, then hotplate baked at 80^0 C for 4 minutes. Electron beam lithography was performed using a JEOL JBX-6300FS system operated at 100 KeV energy, 8 nA beam current, and 500 μm exposure field size. The machine grid used for shape placement was 1 nm, while the beam stepping grid, the spacing between dwell points during the shape writing, was 6 nm. An exposure dose of $2800\mu C/cm^2$ was used. The resist was developed by immersion in 25% tetramethylammonium hydroxide for 4 minutes, followed by a flowing deionized water rinse for 60 s, an isopropanol rinse for 10 s, and then blown dry with nitrogen. The silicon was removed from unexposed areas using inductively coupled plasma etching in an Oxford Plasmalab System 100, with a chlorine gas flow of 20 sccm, pressure of 12 mT, ICP power of 800 W, bias power of 40 W, and a platen temperature of 20^0C, resulting in a bias voltage of 185 V. During etching, chips were mounted on a 100 mm silicon carrier wafer using perfluoropolyether vacuum oil. Figures 4(a) and 4(b) show top view SEM images of a fabricated strip to slot waveguide mode converter and a section of slot waveguide Bragg gratings with internal corrugation width

Optics EXPRESS

of 20 nm described in the modeling and simulation section.

4. Experimental data results and discussion

The characterization of the devices were carried out using a custom-built automated test setup [20] with the automated control software written in Python (http://siepic.ubc.ca/probestation). The input source is an Agilent 86100B tunable laser and the output detectors are Agilent 81635A optical power sensors. The measured wavelength range is 1520-1580 nm in 10 pm steps and the measurement temperature is 25^0C. A polarization maintaining fiber is used to couple TE polarized light from the input laser to the grating couplers [21]. Coupling light into and out of the chip was achieved using a polarization maintaining fiber array. The input power of the laser source is set to 1 mW or 0 dBm.

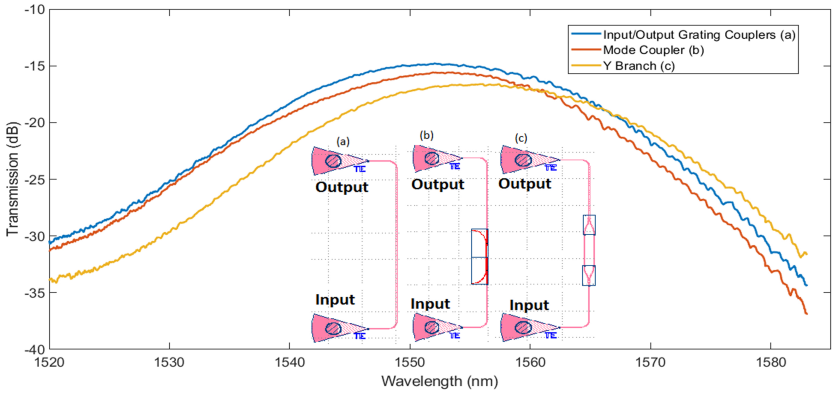

Fig. 5. Measured transmission spectra for input output grating couplers, strip to slot waveguide mode couplers and Y branches connected back to back, which correspond to the kLayout screen capture photonic circuits shown inset as (a), (b), and (c) respectively along with labeled input and output grating couplers.

The input and output grating couplers used to couple light into the photonic circuit have a wavelength dependant transmission as shown in Fig. 5 with least loss at 1555 nm. Also shown in Fig. 5 are measured transmission spectra for strip to slot waveguide mode couplers and Y branches connected back to back with zero path length difference. We can observe that for both these case, the transmission spectra follows a similar uniform profile as the input output grating couplers and we observe no fringes due to Fabry-Perot reflections as result of inserting the mode couplers and Y branches into the photonic circuit.

The transmission spectrum for the slot BG's with ΔW_{in} = 20 nm show a clear stopband with an extinction ratio around 30 dB as shown in Fig. 6. We can observe strong fluctuations in the transmission at the stop band edge from 1520-1530 nm for the slot BG with Λ = 466 nm. This is due to group index mismatch from the slot mode to the slow light mode in the slot BG.This results in high losses as shown in the transmission response of the MZI circuit in Fig. 7, where small fringes of extinction ratio lower than 5 dB are obtained in the wavelength region of 1520-1530 nm. However, at the longer wavelength stopband edge, the fluctuations are minimized due to lower group index mismatch in the transition from slow light to fast light. This can be understood from the photonic band diagram of a 1D periodic structure where the first frequency photonic band corresponding to the higher wavelength stopband edge location has a lower group index dispersion compared to the second frequency photonic band where the lower wavelength stopband edge is present [22]. This causes a more efficient interference between the

Optics EXPRESS

slow light mode and strip waveguide mode resulting in larger fringes with extinction ratio ~ 15 dB at wavelengths near 1555 nm and 1569 nm as shown in Fig. 7.

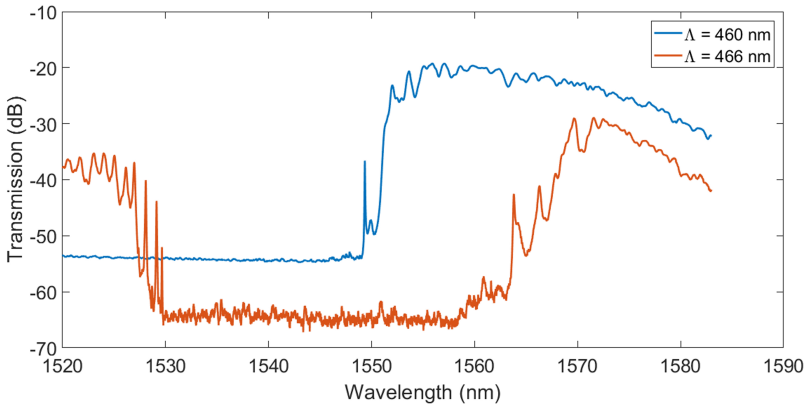

Fig. 6. Measured transmission spectra for slot BG's with ΔW_{in} = 20 nm having Bragg periods of 460 nm and 466 nm.

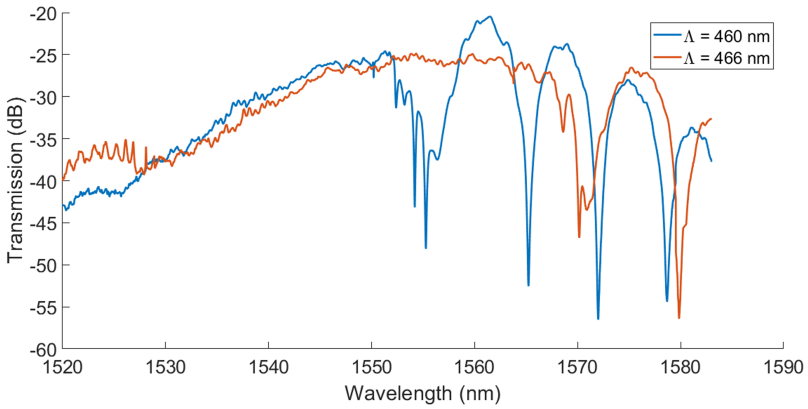

Fig. 7. Measured transmission spectra for the MZI circuits with one arm as strip waveguide and the other arm as slot BG with ΔW_{in} = 20 nm and for Bragg periods of 460 nm and 466 nm.

Using the MZI circuit shown in Fig. 8(b), which has one arm as a slot waveguide obtained by setting ΔW_{in} to 0 and the other arm as a strip waveguide, we observe clear MZI fringes with nearly uniform spacing indicating small variation in the group index of the slot waveguide over the entire wavelength range of 1520-1580 nm. The effect of grating coupler loss which is higher around 1520 nm and 1580 nm can be observed in the transmission spectrum shown in Fig. 8(a). Also shown in Fig. 8(a) is the calculated group index for the slot waveguide from the transmission spectrum data, which is 2.503 at a wavelength of 1553 nm.

The measured MZI transmission spectrum for slot BG with period of 460 nm and internal corrugation width of 20 nm shown in Fig. 7 is analyzed for its slow light properties around 1550 nm as as shown in Fig. 9. We can clearly observe a fast light region with uniform fringe spacing and having a higher contrast ratio between maxima and minima, followed by a slow light region

Optics EXPRESS

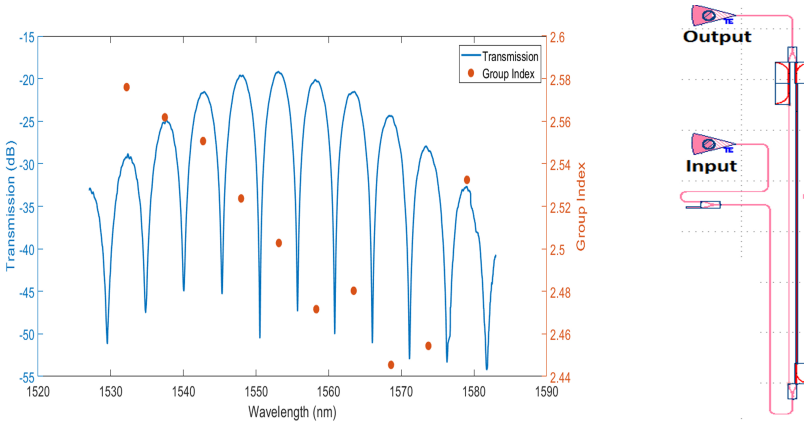

(a) (b)

Fig. 8. (a) Measured transmission spectrum for MZI circuit with one arm as slot waveguide (i.e. with $\Delta W_{in} = 0$) and calculated group index for the slot waveguide. (b) kLayout screen capture of the MZI circuit.

next to the photonic bandgap boundary where fringe minima are closely spaced and have lower contrast between maxima and minima. This is because of interference between higher loss slow propagating wave in the slot waveguide BG arm and light wave from the reference arm strip waveguide which has higher optical power.

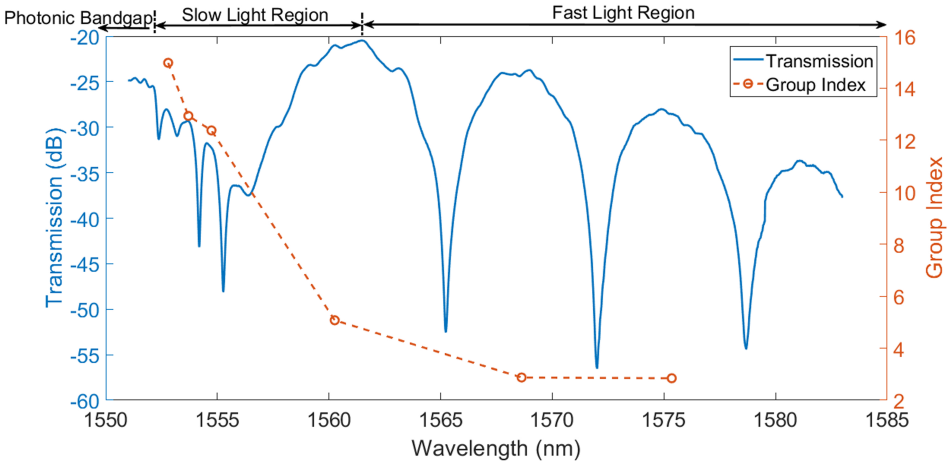

Fig. 9. Measured raw transmission spectra for $\Delta W_{in} = 20$ nm with Bragg period of 460 nm along with calculated group index.

The extracted group index from the measured transmission spectrum is shown in Fig. 9 with a peak group index ~ 15 at 1553 nm respectively which is comparable to the peak group index of ~ 22 at 1563 nm obtained in simulation. Also, we can observe in the slow light region of Fig. 9, a useful extinction ratio of 13.8 dB is obtained with group index of 12.94 at a wavelength of 1554 nm. This is a significant improvement is the extinction ratio in contrast to 2-5 dB obtained for externally corrugated 1D PC slot waveguide for comparable group indices [11]. This translates to lower phase shifter insertion loss as discussed in the photonic circuit simulation section.By

considering the maxima and minima of electric field in the MZI transmission output, an insertion loss of 3.5 dB at 1554.7 nm wavelength where the group index is 12.38 is obtained. Alternatively, one could obtain the slow light phase shifter insertion loss from the normalized transmission spectrum of the slot BG waveguide section. Figure 10(a) shows the normalized version of the measured transmission spectrum data of slot waveguide BG with ΔW_{in} = 20 nm and Bragg period of 460 nm. In the normalized transmission spectrum, effect of the input output grating couplers, Y branches and strip waveguide bends were subtracted out by using the transmission spectrum from a replica photonic circuit which has a straight strip waveguide instead of the slot waveguide BG section as shown in Fig. 10(b). Effect of strip to slot waveguide mode couplers were subtracted out using the measurement data shown in Fig. 5 leaving only the transmission spectrum response of the slot waveguide Bragg section as shown in the normalized data plot in Fig. 10(a). Figure 11 shows combined plot of the normalized spectrum in Fig. 10(a) and the corresponding measured MZI spectrum in Fig. 9. We can observe that at the wavelength corresponding to the group index of 12.38 in the slow light region, a low insertion loss of ~ 2.9 dB is obtained from the normalized spectrum data.

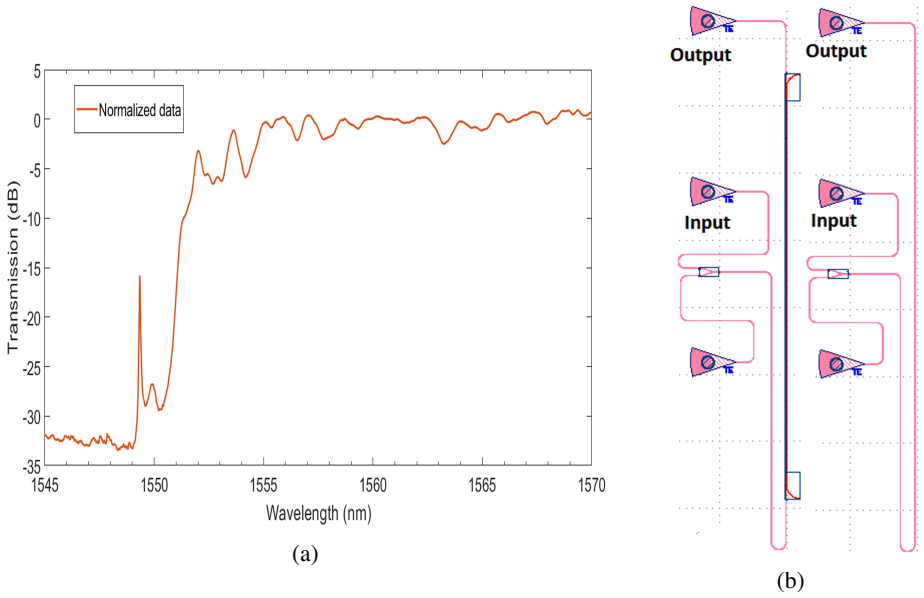

(a) (b)

Fig. 10. (a) Measured transmission output spectrum and normalized data for slot waveguide BG with ΔW_{in} = 20 nm and Bragg period of 460 nm. (b) kLayout screen capture of photonic circuits with the slot wave BG section and a reference straight strip waveguide section to obtain the normalized data plot.

From Fig. 11, we can observe that for the wavelength region 1553-1555 nm , one obtains slow light with group indices of 12-13 and a low insertion loss of 2.906 dB. Slow light coupling loss determined from 3D FDTD simulation of direct coupling between slot waveguide and the slot waveguide BG is ~ 1.5 dB. This gives a slow light propagation loss of ~ 5.1 dB/mm near 1555 nm wavelength. To the best of our knowledge , this is the lowest reported slow light propagation loss in 1D photonic crystal slot waveguides.

The measurement derived results and simulation results confirm that slow light with low loss propagation is possible with internally corrugated slot waveguide Bragg gratings. Internal corrugated slot waveguide BG design with ΔW_{in} = 20 nm have slow light group indices of 12-13 with a comparatively low phase shifter insertion loss of 3-5 dB as shown in Fig. 11. Both

Optics EXPRESS

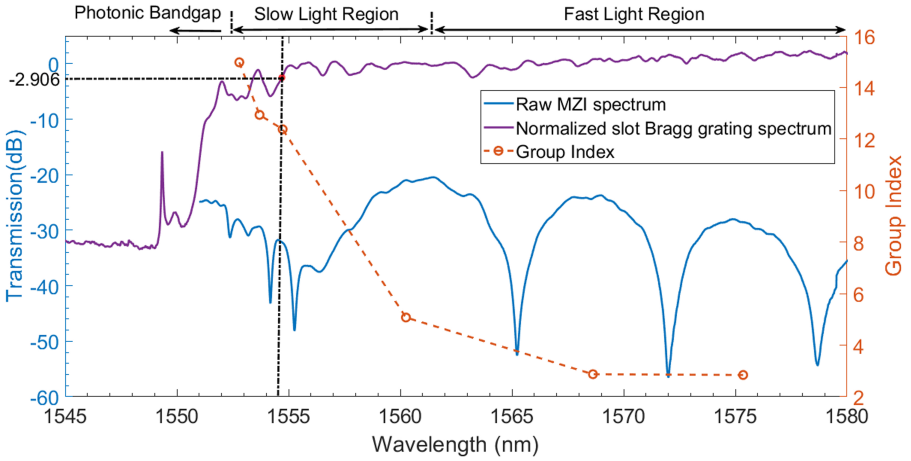

Fig. 11. Combined plot of phase shifter insertion loss and group index along with the measured transmission spectra for slot waveguide BG with ΔW_{in} = 20 nm and Bragg period of 460 nm.

simulation and measurement data have a group index in the range ~10-20 in the slow light region and internal corrugation provides a more efficient interaction compared to an externally corrugated 1D PC slot waveguide where a propagation loss of 15 dB/mm was obtained for a similar group index [11]. The insertion loss could be further reduced by introducing a step taper [11] in the slot BG section thereby providing better coupling from slot mode to slow light mode.

Although the current designs were fabricated using e-beam lithography which is a prototyping tool, the device dimensions considered in the design are compatible with deep ultra violet (UV) CMOS fabrication. The grating corrugations are on the sidewalls of the slot waveguide arms and therefore can be defined in single lithography step. Slot waveguide Bragg gratings with 10 nm width corrugations have been fabricated using CMOS fabrication tools [9]. The critical dimension for fabrication in designs considered here is the minimum separation gap between the slot waveguide arms, which is 80 nm for the slot waveguide BG with ΔW_{in} = 20 nm, as the slot gap is 100 nm. It has been shown that with advanced 193 nm deep UV immersion lithography, photonic devices with feature sizes including narrow trenches of 50 nm width can be fabricated [23]. Therefore, the considered slot waveguide BG designs are CMOS foundry compatible.

4.1. Device application potential

A key application of silicon slot waveguides is as a phase shifter for high speed, low voltage electro-optic modulator applications [3–6]. The advantage of slot waveguide over conventional low loss strip waveguides for this application is that slot waveguide geometry enables a stronger electric field as the electrodes can be connected to the silicon slot waveguide arms allowing for electrode spacing in the range of ~ 100 nm as compared to several micrometers which is the case for strip waveguide phase shifters. This results in at least an order of magnitude improvement in the modulator device figure of merit $V_\pi.L$ compared to similar modulators using strip waveguide phase shifters which generally have a $V_\pi.L$ over 1 V.cm [24] .

Polymer materials exhibit low loss of below 0.1 dB/cm in communication window wavelengths, possess refractive index in the range of 1.5-1.7 and a strong Pockels coefficient [25] making them an attractive material for hybrid silicon-based electro-optic modulator applications [26].

Optics EXPRESS

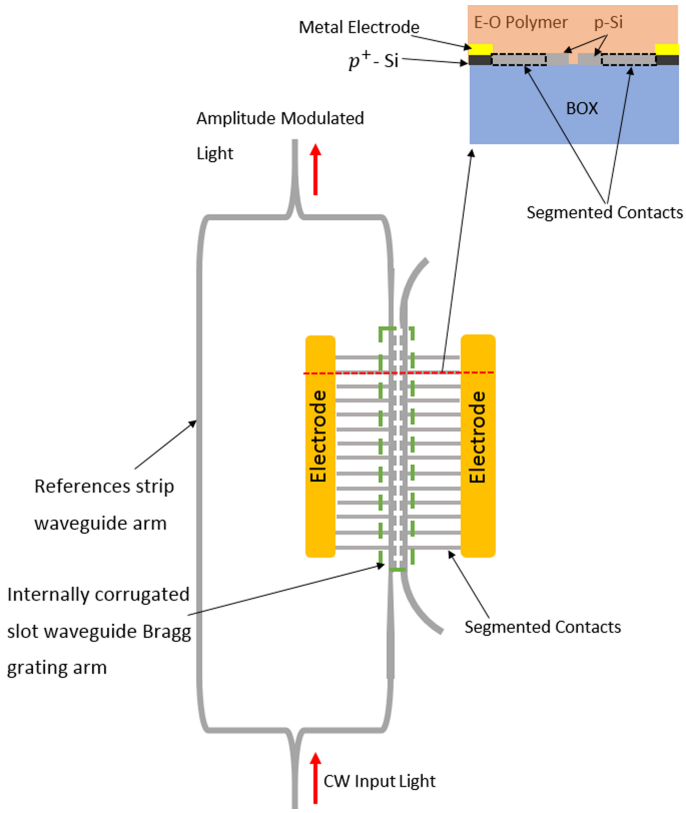

Fig. 12. Schematic of Mach Zehnder modulator (MZM) using the internally corrugated slot waveguide Bragg gratings and cross section view in the slot waveguide BG arm.

Modulation is achieved using the linear Pockels effect in the electro optic polymer medium. The schematic for an electro-optic modulator using the internally corrugated slot waveguide BG in an MZM configuration is shown in Fig. 12. The device schematic is similar to the demonstrated MZM in [11] and MZI structure based electro-magnetic wave sensor in [27] where electro-optic polymer SEO125 from Soluxra LLC was used as the active medium. The proposed design uses the same narrow contacts with sub wavelength period as in [27] to provide electrical connection and achieve voltage drop across the slot with low optical loss. Segmented contacts with a sub wavelength period of 300 nm and segment width of 100 nm as in the demonstrated polymer clad electro-optic modulator [5] are considered in this design. Considering doping concentration of $10^{17}/cm^3$ for the silicon slot waveguide and segmented contact sections, propagation loss of the doped segmented slot waveguide section is estimated to be 10 dB/cm [28].

Interaction factor is an important parameter for modulator applications as it quantifies the strength of interaction between light in the waveguide and the electro-optic medium. The phase shift experienced by an optical wave depends on this interaction factor and is given as [29],

$$\Delta\phi = \Gamma \Delta n k_0 L \tag{4}$$

In Eq. (4), Γ is interaction factor of the waveguide, Δn is the induced material refractive index change, k_0 is the free space wave number and L is length of the phase modulator section. We can observe from Eq. (4) that having a phase modulator section with a higher interaction factor

would make the electro-optic device more phase sensitive for the same material refractive index change and therefore more energy efficient. The interaction factor varies inversely with the group velocity [29] and is therefore directly proportional to the group index. Using this relationship, the interaction factor for slot waveguide Bragg gratings can be estimated as follows,

$$\Gamma(\lambda) = \left(\frac{n_g(\lambda)}{n_{g(slot)}(\lambda)}\right).\Gamma_{slot}(\lambda) \tag{5}$$

Here, $\Gamma_{slot}(\lambda)$ is the interaction factor for the nominal slot waveguide which simplifies to the confinement factor, $n_{g(slot)}(\lambda)$ and $n_g(\lambda)$ are the group indices of the slot waveguide and slot waveguide BG at the corresponding wavelength respectively. The material refractive index change due to Pockels effect is proportional to the applied electric field (E) as [29] ,

$$\Delta n = \frac{-1}{2}(n^3 r_{33} E)\,,\; E = \frac{V}{g} \tag{6}$$

Here, n is the refractive index of the slot material which is the electro-optic polymer, r_{33} is electro-optic polymer's Pockels coefficient inside the slot, V is the applied voltage and g is the gap between the electrical contacts.

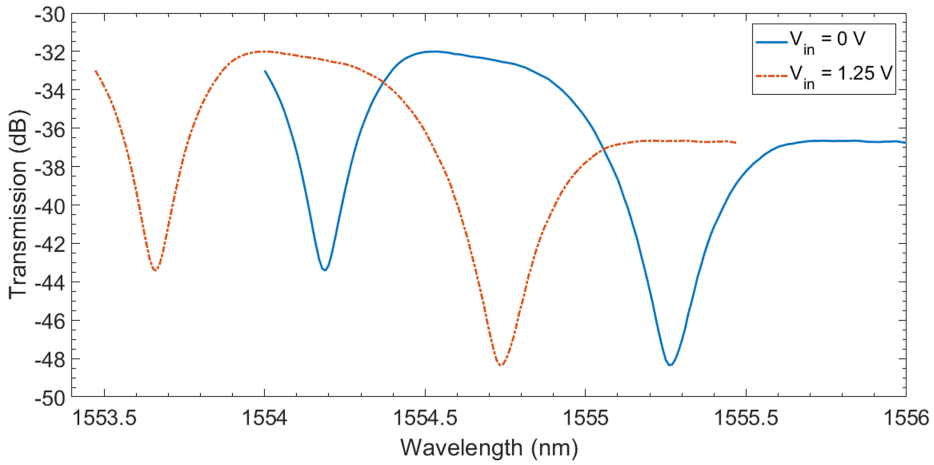

Fig. 13. Predicted transmission spectra in the slow light region for the Mach Zehnder modulator shown in Fig. 12.

The electro-optic polymer SEO 125 has a bulk r_{33} of ~ 100 pm/V , refractive index of 1.63 at 1550 nm and a low optical loss [12]. It has been used to demonstrate a slow light enhanced effective r_{33} of 490 pm/V [11] in a 150 nm wide slot, which corresponds to a material r_{33} of ~ 68 pm/V in the slot region taking the slow down factor (S) as 7.14 ($S = n_g/n_\phi = 20/2.8 = 7.14$). Using the same electro-optic polymer SEO125 as the cladding material in the design shown in Fig. 12 along with its material parameters and a slow light enhanced interaction factor of 1.659 for the designed slot waveguide BG, an excellent $V_\pi L$ of 0.317 V.mm is obtained. The change in cladding from silica (n=1.44) to the electro-optic polymer SEO 125 (n=1.63) is compensated by changing the Bragg period from 460 nm to 417 nm so that the phase shifter length is now $L = 600 \times 0.417 = 250.2$ μm and measured slow light region as shown in Fig. 11 remains around 1555 nm. The transmission spectrum including a bias of 1.25 V is shown in Fig. 13. In this preliminary analysis, an average value of 100 nm is used for g. This is because a fluctuation of 40 nm across the Bragg period of 417 nm due to internal corrugations corresponds to 0.16 %

Optics EXPRESS

variation in g over the entire phase shifter length of 250.2 microns. We can observe from Fig. 13 that an input voltage of 1.25 V is close to the V_π voltage for the MZM with a useful extinction ratio of 16 dB at 1554.7 nm. Taking the worst case scenario of 120 nm as the slot gap through out the phase shifter, still gives an attractive $V_\pi L$ of 0.382 V.mm corresponding to a V_π voltage of 1.51 V.

Using the phase shifter figure of merit ($f = \sigma.n_g.L_{3dB}$) [11] in the slow light wavelength region of 1555 nm, a value of $f = 0.37 \times 12.38 \times 0.588 \sim 2.69$ is obtained for the slot BG waveguide design with $\Delta W_{in} = 20$ nm. Here σ is the optical mode confinement factor in the slot region that overlaps with the applied DC electric field, n_g is the group index of the optical mode and L_{3dB} is the phase shifter length in mm for 3 dB propagation loss. Table 1 summarizes and compares different slot waveguide based phase shifters in terms of f and the electro-optic modulator figure of merit $V_\pi.L$.

Table 1. Comparison of Slot Waveguide-Based Phase Shifter Structures

Phase Shifter Structure	**Propagation loss (dB/mm)**	**f = $\sigma n_g L_{3dB}$**	**V_π.L (V.cm)**	**Phase Shifter length (mm)**
Strip loaded slot waveguide [3]	4	0.45	0.052	1
2D PC Slot waveguide [12]	20	1.05	0.0282	0.3
1D PC Slot waveguide [11]	15	1.40	0.91	0.2
Proposed slot BG waveguide ($\Delta W_{in} = 20$ nm)	5.1	2.69	0.031	0.25

Although conventional slot waveguide geometries have potential for lowering propagation loss through improved fabrication processes, they are limited in terms of lowering the modulator figure of merit $V_\pi.L$ and device size as they rely on a polymer medium with high a Pockels coefficient to achieve large in-device r_{33} values as in [3] where an in-device r_{33} of 230 pm/V was achieved using SOH polymers. Slot waveguides embedded with photonic crystals on the other hand provide a slow light enhanced in-device r_{33} in the slow light wavelength region, resulting in lower $V_\pi.L$ with compact phase shifter lengths in the range of $\sim$ 100's of μm as shown in Table 1. This is at the expense of a narrow operational bandwidth which is $\sim$ 2 nm for the proposed design but which can be improved using band engineering [12]. 1D PC slot waveguide have lower loss slow light compared to 2D PC slot waveguide and can still provide comparable $V_\pi.L$ to the 2D PC slot waveguide modulator. The proposed internally corrugated slot BG waveguide has a predicted $V_\pi.L$ of only 0.031 V.cm considering an in-slot r_{33} of 68 pm/V, which has been accomplished in a 1D PC slot waveguide geometry [11]. The internally corrugated slot BG discussed here with its higher phase shifter efficiency and capability of low $V_\pi.L$ electro-optic modulation, makes it useful for other applications which require an efficient phase shifter section as in electromagnetic wave sensors [27] or biosensors [7, 8]. A detailed analysis for these applications is beyond the scope of this paper.

Optics EXPRESS

5. Summary and conclusion

Slot waveguide BG with internal corrugation design has been analyzed for its slow light properties in 1520-1580 nm wavelength range in simulation and in experiment. Slot BG with internal corrugations provide stronger and more efficient interaction than external corrugations. Group indices of 12-13 and insertion loss of 3-5 dB for internally corrugated slot waveguide Bragg gratings were extracted out through experimentally obtained transmission spectra.This improved interaction between the periodic corrugations and the slot mode results in a enhanced phase shifter figure of merit. A minimum slow light propagation loss of ~ 5.1 dB/mm is obtained experimentally which to the best of our knowledge is the lowest reported slow light propagation loss for slot waveguides using a 1D photonic crystal structure. The application of a slot BG with ΔW_{in} = 20 nm as a phase shifter in a electro-optic MZM has been analyzed with a calculated $V_{\pi}.L$ of only 0.031 V.cm. In conclusion, slot BG waveguide with internal corrugations being easier to fabricate than 2D PC slot waveguides can provide slow light enhancements with low loss for practical high performance electro-optic modulator applications and potentially sensing applications.

Funding

Natural Sciences and Engineering Research Council of Canada (NSERC); Program Applied Science in Photonics and Innovative Research in Engineering (ASPIRE);European Regional Development Fund in the IT4Innovations National Supercomputing Center-Path to Exascale Project (project number CZ.02.1.01/0.0/0.0/16_013/0001791) within the Operational Programme Research, Development and Education.

Acknowledgments

We acknowledge the edX UBCx Phot1x Silicon Photonics Design, Fabrication and Data Analysis course, which is supported by the Natural Sciences and Engineering Research Council of Canada (NSERC) Silicon Electronic-Photonic Integrated Circuits (SiEPIC) Program. The devices were fabricated by Richard Bojko at the University of Washington Washington Nanofabrication Facility, part of the National Science Foundation's National Nanotechnology Infrastructure Network (NNIN). Measurements were performed through the automated test setup at The University of British Columbia.We thank Professor J. Pistora from the Nanotechnology Center, VSB-Technical University of Ostrava for valuable suggestions and support of this work. We acknowledge CMC Microsystems for access to design software in particular, Lumerical Solutions, Inc.,Photon Design, Mathworks, Python, and KLayout.

References

1. Q. Xu, V. R. Almeida, R. R. Panepucci, and M. Lipson, "Experimental demonstration of guiding and confining light in nanometer-size low-refractive-index material," Opt. Lett. **29**, 1626–1628 (2004).
2. D. Dai, J. Bauters, and J. E. Bowers, "Passive technologies for future large-scale photonic integrated circuits on silicon: Polarization handling, light non-reciprocity and loss reduction," Light Sci. Appl. **1**, 1–12 (2012).
3. R. Palmer, S. Koeber, D. L. Elder, M. Woessner, W. Heni, D. Korn, M. Lauermann, W. Bogaerts, L. Dalton, W. Freude, J. Leuthold, and C. Koos, "High-speed, low drive-voltage silicon-organic hybrid modulator based on a binary-chromophore electro-optic material," J. Light. Technol. **32**, 2726–2734 (2014).
4. M. Hochberg, T. Baehr-Jones, G. Wang, J. Huang, P. Sullivan, L. Dalton, and A. Scherer, "Towards a millivolt optical modulator with nano-slot waveguides," Opt. Express **15**, 8401 (2007).
5. T. Baehr-Jones, B. Penkov, J. Huang, P. Sullivan, J. Davies, J. Takayesu, J. Luo, T. D. Kim, L. Dalton, A. Jen, M. Hochberg, and A. Scherer, "Nonlinear polymer-clad silicon slot waveguide modulator with a half wave voltage of 0.25 V," Appl. Phys. Lett. **92**, 23–25 (2008).
6. L. Alloatti, R. Palmer, S. Diebold, K. P. Pahl, B. Chen, R. Dinu, M. Fournier, J. M. Fedeli, T. Zwick, W. Freude, C. Koos, and J. Leuthold, "100 GHz silicon-organic hybrid modulator," Light Sci. Appl. **3**, 5–8 (2014).
7. Q. Liu, X. Tu, K. W. Kim, J. S. Kee, Y. Shin, K. Han, Y. J. Yoon, G. Q. Lo, and M. K. Park, "Highly sensitive Mach-Zehnder interferometer biosensor based on silicon nitride slot waveguide," Sensors Actuators, B Chem. **188**, 681–688 (2013).

Optics EXPRESS

8. X. Wang, J. Flueckiger, S. Schmidt, S. Grist, S. T. Fard, J. Kirk, M. Doerfler, K. C. Cheung, D. M. Ratner, and L. Chrostowski, "A silicon photonic biosensor using phase-shifted Bragg gratings in slot waveguide," J. Biophotonics **828**, 821–828 (2013).
9. X. Wang, N. A. F. Jaeger, J. Flueckiger, S. Grist, and L. Chrostowski, "Silicon photonic slot waveguide Bragg gratings and resonators," Opt. Express **21**, 19029 (2013).
10. F. Riboli, P. Bettotti, and L. Pavesi, "Band gap characterization and slow light effects in one dimensional photonic crystals based on silicon slot-waveguides," Opt. Express **15**, 11769 (2007).
11. H. Yan, C.-J. Chung, H. Subbaraman, S. Chakravarty, H. Subbaraman, Z. Pan, S. Chakravarty, and R. T. Chen, "One-dimensional photonic crystal slot waveguide for silicon-organic hybrid electro-optic modulators," Opt. Lett. **41**, 5466 (2016).
12. X. Zhang, C.-J. Chung, A. Hosseini, H. Subbaraman, J. Luo, A. K.-Y. Jen, R. L. Nelson, C. Y.-C. Lee, and R. T. Chen, "High Performance Optical Modulator Based on Electro-Optic Polymer Filled Silicon Slot Photonic Crystal Waveguide," J. Light. Technol. **34**, 2941–2951 (2015).
13. X. Wang, C.-Y. Lin, S. Chakravarty, J. Luo, A. K.-Y. Jen, and R. T. Chen, "Effective in-device r_33 of 735 pm/V on electro-optic polymer infiltrated silicon photonic crystal slot waveguides," Opt. Lett. **36**, 882 (2011).
14. A. Di Falco, M. Massari, M. G. Scullion, S. A. Schulz, F. Romanato, and T. F. Krauss, "Propagation losses of slotted photonic crystal waveguides," IEEE Photonics J. **4**, 1536–1541 (2012).
15. W. Bogaerts, M. Fiers, and P. Dumon, "Design Challenges in Silicon Photonics," IEEE J. Sel. Top. Quantum Electron. **20** (2014).
16. L. Chrostowski, Z. Lu, J. Flueckiger, X. Wang, J. Klein, A. Liu, J. Jhoja, and J. Pond, "Design and simulation of silicon photonic schematics and layouts," in "Silicon Photonics Photonic Integr. Circuits V," (International Society for Optics and Photonics, 2016), p. 989114.
17. A. Brimont, A. M. Gutierrez, M. Aamer, D. J. Thomson, F. Y. Gardes, J. Fedeli, G. T. Reed, J. Marti, and P. Sanchis, "Slow-Light-Enhanced Silicon Optical Modulators Under Low-Drive-Voltage Operation," IEEE Photonics J. **4**, 1306–1315 (2012).
18. Q. Fang, J. F. Song, T.-Y. Liow, H. Cai, T.-Y. Liow, G. Q. Lo, and D.-L. Kwong, "Ultralow Power Silicon Photonics Thermo-Optic Switch With Suspended Phase Arms," IEEE Photonics Technol. Lett. **23**, 525–527 (2011).
19. R. J. Bojko, T. Baehr-Jones, Y. Aida, L. He, M. Hochberg, and J. Li, "Electron beam lithography writing strategies for low loss, high confinement silicon optical waveguides," Journal of Vacuum Science & Technology B, Nanotechnology and Microelectronics: Materials, Processing, Measurement, and Phenomena **29**, 063F09 (2011).
20. L. Chrostowski and M. Hochberg, *Silicon Photonics Design: from devices to systems* (Cambridge University Press, 2015).
21. Y. Wang, X. Wang, J. Flueckiger, H. Yun, W. Shi, R. Bojko, N. A. F. Jaeger, and L. Chrostowski, "Focusing sub-wavelength grating couplers with low back reflections for rapid prototyping of silicon photonic circuits," Opt. Express **22**, 20652–20662 (2014).
22. B. Saleh and M. Teich, *Fundamentals of Photonics* (John Wiley and Sons Inc., 2007).
23. S. K. Selvaraja, G. Winroth, S. Locorotondo, G. Murdoch, A. Milenin, C. Delvaux, P. Ong, S. Pathak, W. Xie, G. Sterckx, G. Lepage, D. Van Thourhout, W. Bogaerts, J. Van Campenhout, and P. Absil, "193Nm Immersion Lithography for High-Performance Silicon Photonic Circuits," in "SPIE 9052, Optical Microlithography XXVII," , vol. 9052 (2014), vol. 9052, p. 90520F.
24. H. Tazawa, Y.-h. Kuo, I. Dunayevskiy, J. Luo, A. K. Jen, H. R. Fetterman, W. H. Steier, and L. Fellow, "Ring Resonator-Based Electrooptic Polymer Traveling-Wave Modulator," J. Lightwave Technol. **24**, 3514–3519 (2006).
25. B. Hong Ma, A. K-Y Jen, and L. R. Dalton, "Polymer-Based Optical Waveguides: Materials, Processing, and Devices," Adv. Mater. **14**, 1339–1365 (2002).
26. X. Zhang, A. Hosseini, X. Lin, H. Subbaraman, and R. T. Chen, "Polymer-based hybrid-integrated photonic devices for silicon on-chip modulation and board-level optical interconnects," IEEE J. Sel. Top. Quantum Electron. **19** (2013).
27. C.-J. Chung, X. Xu, Z. Pan, F. Mokhtari-Koushyar, R. Wang, H. Yan, and R. T. Chen, "Silicon-Based Hybrid Integrated Photonic Chip for Ku band Electromagnetic Wave Sensing," J. Lightwave Technol. **36**, 1568–1575 (2018).
28. G. Wang, T. Baehr-Jones, M. Hochberg, and A. Scherer, "Design and fabrication of segmented, slotted waveguides for electro-optic modulation," Appl. Phys. Lett. **91**, 2005–2008 (2007).
29. J.-M. Brosi, C. Koos, L. C. Andreani, M. Waldow, W. Freude, and J. Leuthold, "High-speed low-voltage electro-optic modulator with a polymer-infiltrated silicon photonic crystal waveguide," Opt. Express **16**, 4177 (2008).